The Astrophysical Journal Letters, 775:L15 (6pp), 2013 September 20 doi:10.1088/2041-8205/775/1/L15
© 2013. The American Astronomical Society. All rights reserved. Printed in the U.S.A.

BREAKING THE OBSCURING SCREEN: A RESOLVED MOLECULAR OUTFLOW IN A BURIED QSO

David S. N. Rupke[1] and Sylvain Veilleux[2]
[1] Department of Physics, Rhodes College, Memphis, TN 38112, USA; drupke@gmail.com
[2] Department of Astronomy and Joint Space-Science Institute, University of Maryland, College Park, MD 20742, USA
Received 2013 July 3; accepted 2013 August 21; published 2013 September 4

ABSTRACT

We present Keck laser guide star adaptive optics observations of the nearby buried quasi-stellar object (QSO) F08572+3915:NW. We use near-infrared integral field data taken with the OH-Suppressing Infra-Red Imaging Spectrograph to reveal a compact disk and molecular outflow using Paα and H_2 rotational-vibrational transitions at a spatial resolution of 100 pc. The outflow emerges perpendicular to the disk into a bicone of one-sided opening angle 100° up to distances of 400 pc from the nucleus. The integrated outflow velocities, which reach at least -1300 km s^{-1}, correspond exactly to those observed in (unresolved) OH absorption, but are smaller (larger) than those observed on larger scales in the ionized (neutral atomic) outflow. These data represent a factor of >10 improvement in the spatial resolution of molecular outflows from mergers/QSOs, and plausibly represent the early stages of the excavation of the dust screen from a buried QSO.

Key words: galaxies: evolution – galaxies: ISM – galaxies: kinematics and dynamics – ISM: jets and outflows – quasars: general

Online-only material: color figures

1. INTRODUCTION

Wide angle, large scale outflows in quasi-stellar objects (QSOs) that are driven by black hole accretion energy are a key element of models of major galaxy mergers. In long-standing merger models, such outflows act as feedback on star formation and active galactic nuclei (AGNs). Furthermore, they may transform QSOs buried in dusty molecular disks into true QSOs by "breaking the obscuring screen" of dust (e.g., Sanders et al. 1988; Hopkins et al. 2005).

Large scale, AGN-driven outflows in major mergers have recently been discovered in the ionized, neutral, and molecular gas phases. In the ionized and neutral phases, high velocity outflows in nearby ultraluminous infrared galaxies (ULIRGs) show evidence for acceleration by an AGN in those galaxies where one is present (Rupke & Veilleux 2011; Westmoquette et al. 2012; Rupke & Veilleux 2013, hereafter RV13). The mechanical luminosities of these outflows (10^{43} erg s^{-1}, and $0.002 - 004L_{\rm AGN}$) are inconsistent with driving by a starburst alone but consistent with recent models of AGN feedback (Hopkins & Elvis 2010; Rupke & Veilleux 2011; RV13). The peak velocities in systems that contain an AGN are in the range 1500–3500 km s^{-1}, while the velocities in galaxies without an AGN peak near 1000 km s^{-1} (RV13).

Outflows in mergers and QSOs also have a molecular gas phase, as observed in far-infrared (FIR) *Herschel* spectra (Fischer et al. 2010; Sturm et al. 2011; Veilleux et al. 2013). OH absorption lines show velocities over 1000 km s^{-1} in some galaxies containing an AGN. In several major mergers and/or QSOs, extended, high-velocity CO emission is also observed (Feruglio et al. 2010; Aalto et al. 2012; Cicone et al. 2012, 2013). This gas has velocities up to 800–1000 km s^{-1}, and the sizes of these outflows are $\gtrsim$1 kpc. However, these data were obtained with beam sizes similar to or larger than the inferred spatial extent of the CO emission.

In this Letter, we present integral field spectroscopy (IFS), aided by laser guide star adaptive optics, of the major merger F08572+3915. This interacting system shows high velocity, large scale outflows in neutral, ionized, and molecular gas (Sturm et al. 2011; RV13; Cicone et al. 2013). The FIR luminosity is concentrated in the northwest (NW) nucleus of the system and is powered predominantly by a QSO (Soifer et al. 2000; Armus et al. 2007; Veilleux et al. 2009a), which is heavily obscured at all wavelengths (see the detailed discussion and references in Section 4.1.1 of RV13).

The spatial resolution of these observations is a factor of seven higher than in seeing-limited optical observations (0.″6 seeing; RV13), and a factor ∼30 higher than in millimeter observations (3.″1×2.″7 beam; Cicone et al. 2013). We can thereby probe the spatial structure of the outflow, using near-infrared (NIR) recombination lines and H_2 rotational-vibrational lines, at 100 pc scales. NIR H_2 lines are an excellent tracer of the molecular phase in the M82 wind (Veilleux et al. 2009b). 100 pc approaches the scales at which AGN energy may couple to the outflow (e.g., similar to the radial location of some UV and X-ray absorbers; Crenshaw & Kraemer 2012).

In Section 2, we discuss the observations and data analysis. We present the results in Section 3, and discuss them in Section 4.

2. OBSERVATIONS AND DATA ANALYSIS

We observed F08572+3915:NW using the OH-Suppressing Infra-Red Imaging Spectrograph (OSIRIS; Larkin et al. 2006) on Keck I on UT 2013 January 31. We used the 0.″035 lenslet array and the Kbb filter to achieve spectral coverage of 1.97 to 2.38 μm. We took eight 900 s on-source exposures interleaved with two 900 s sky frames and dithered to achieve a mosaiced field of view (FOV) of 1.″0 × 2.″9. The A0V star HD 95126 served as a telluric standard.

We used v3.2 of the OSIRIS pipeline to sky subtract each on-source exposure and produce a reduced data cube. We then manually aligned the exposures by fitting the galaxy nucleus. We used the pipeline to mosaic the data, combining the

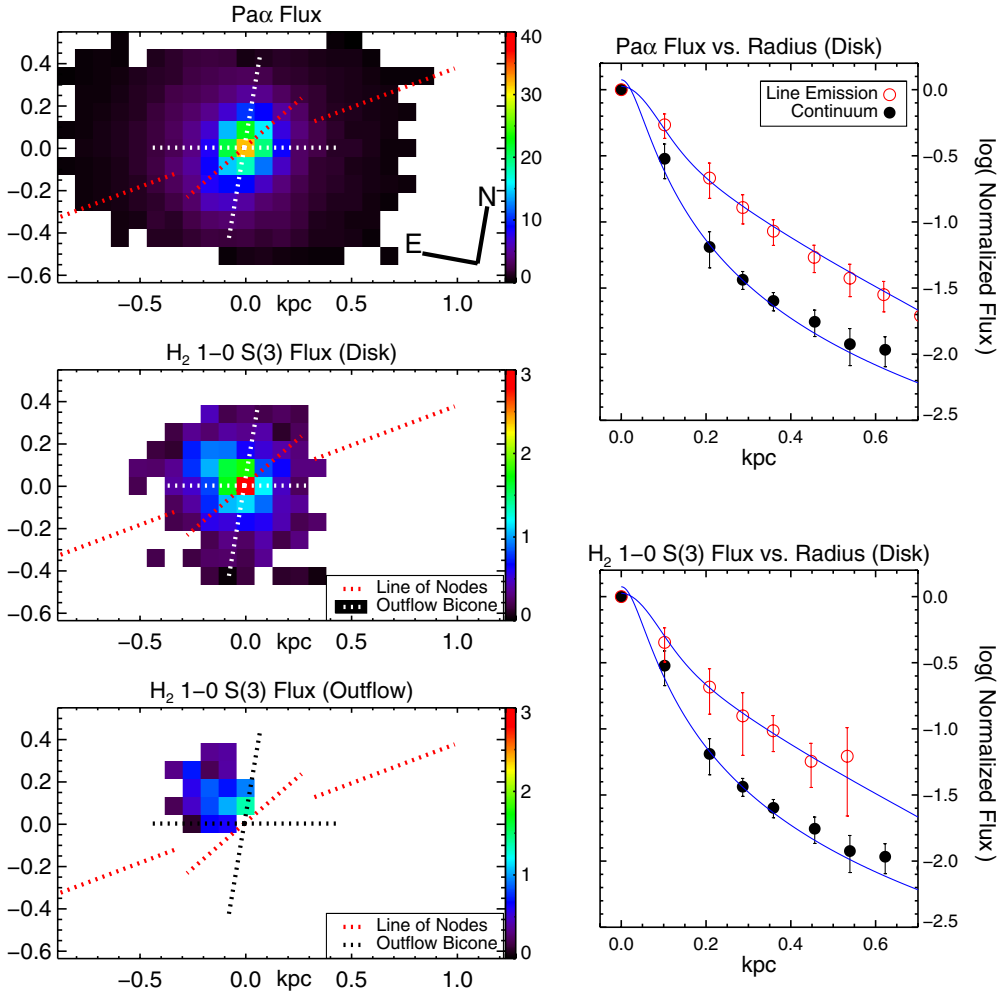

Figure 1. Left: flux maps of the gas disk and outflow in F08572+3915:NW, in units of 10^{-16} erg s^{-1} cm^{-2}. The top two maps shows Paα and H_2 1−0 S(3) in the disk and the bottom map shows H_2 1−0 S(3) in the outflow. The red dotted lines show the approximate lines of nodes of the inner (140° east of north) and outer (120°) disks, while the black and white dotted lines outline a possible biconical shape for the wind (of one-sided opening angle 100°). (For comparison, continuum and dust images appear in Figure 4.) Right: flux vs. radius in 0.″07 radial bins. Black filled circles show the 2.0–2.2 μm continuum; red open circles show line emission; and error bars represent dispersion. The blue line through the continuum data is a Moffat fit (FWHM = 0.″09). The blue line through the emission line data is a Gaussian + exponential model.

(A color version of this figure is available in the online journal.)

exposures with the MEANCLIP algorithm and a 2.35σ threshold for rejection. We removed hydrogen lines from the telluric spectrum and normalized it with a 9480 K blackbody before dividing the science data by the telluric spectrum. We binned the data cube into 0.″07 square spaxels. To flux calibrate the data, we compared Vega flux densities (Tokunaga & Vacca 2005) to the measurements of our telluric standard, with the normalization between the two stars determined from 2MASS fluxes.

We fitted the data using UHSPECFIT (Rupke et al. 2010). In each spaxel we simultaneously fitted a third order polynomial and a set of Gaussians to the continuum and emission lines, respectively. The emission lines we fitted were Paα, Brδ, Brγ, He I 1.87 μm, He I 2.06 μm, H_2 1−0 S(3), H_2 1−0 S(2), and H_2 1−0 S(1). We used one Gaussian for the recombination lines and one or two for the H_2 lines. The recombination lines were constrained to have the same redshift and linewidth within each spaxel. The same was done for the molecular lines, though this redshift and linewidth could be different from those of the recombination lines. H II components were required to be detected in Paα at the 3σ level, while H_2 components were required to be detected in at least two separate lines at 3σ or an individual line at 5σ. The second velocity component in the molecular lines, if present in a given spaxel at a significant level, was found to be always blueshifted, broader, and weaker in peak flux than the first component. For this broad component, the fit was constrained only by the S(3) and S(1) lines, as the S(2) line was not detected in integrated spectra (Section 2). Furthermore, this second component was allowed in a few spaxels on the basis of its clear presence after visual inspection, even if it was slightly under the quantitative significance criterion.

A radial Moffat fit to the 2.0–2.2 μm continuum data yielded a FWHM of 0.″09, corresponding to 100 pc (Figure 1). The fit accounts for sampling effects in the central spaxel, and is consistent with the continuum being an unresolved point source. Scoville et al. (2000) also find that the nucleus of this system is unresolved in the NIR with the *Hubble Space Telescope* (*HST*).

3. RESULTS

The H II and H_2 lines in F08572+3915:NW reveal the presence of a compact gas disk. Figure 1 shows flux maps in Paα and H_2 1−0 S(3) and binned radial profiles. The data are consistent with a compact source plus an extended component.

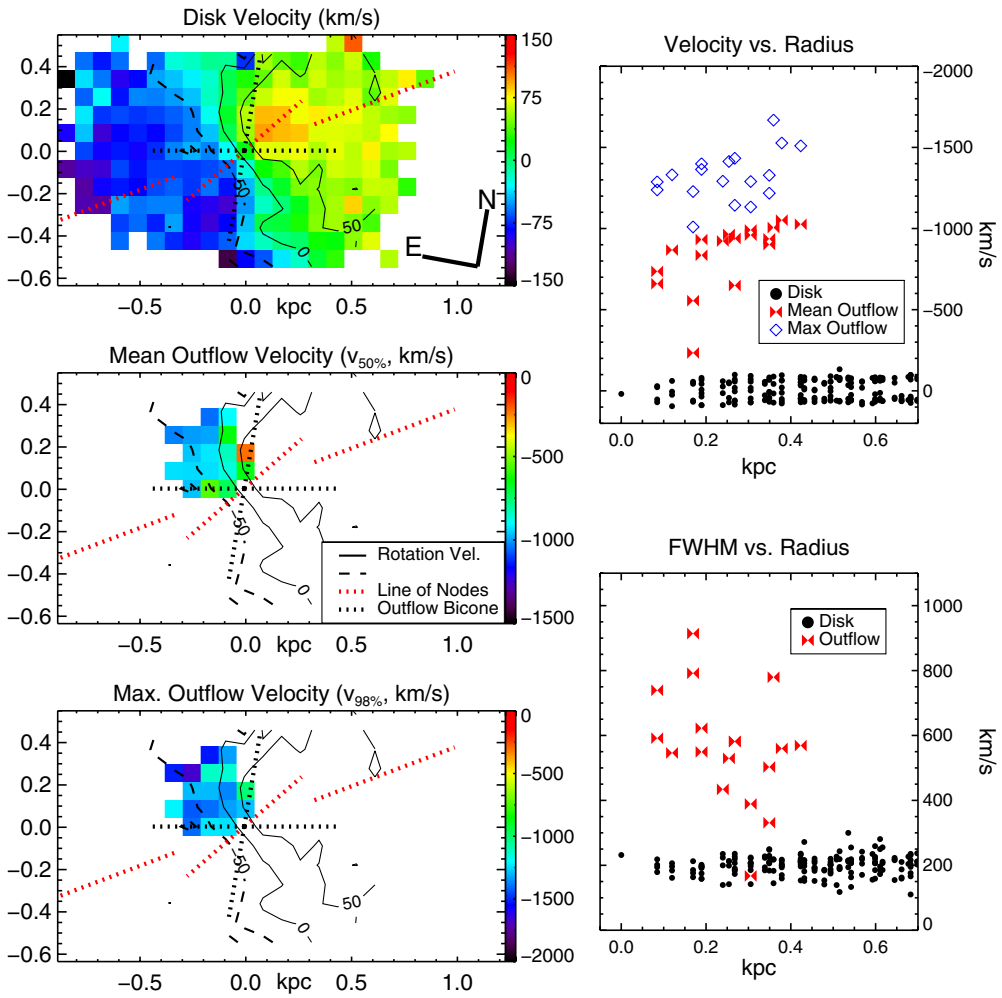

Figure 2. Left: velocity maps of rotation and outflow in F08572+3915:NW, with respect to $z = 0.0583$. From top to bottom: ionized gas rotation, mean outflow velocity ($v_{50\%}$) in H_2, and maximum outflow velocity ($v_{98\%}$) in H_2. The red and black dotted lines are the same as in Figure 1. The blueshifted component extends along the minor axis of the nuclear disk. Right: velocity and FWHM vs. radius. Black filled circles represent velocity and FWHM of rotating components (Paα), red filled hourglasses show mean outflow velocity and outflow FWHM (H_2), and blue open diamonds show maximum outflow velocity. The outflow is more blueshifted with increasing radius, while the FWHM declines.

(A color version of this figure is available in the online journal.)

We model this superposition in radial space as a Gaussian (FWHM $\sim$ 100 pc) plus an exponential (scale length $\sim$200 pc), after convolving each with the continuum point spread function. In our model, the Gaussian and exponential have a peak flux ratio of 3:1. This model, though azimuthally averaged, illustrates that the central gas concentration is compact. If 100–200 pc is a characteristic radius for the nuclear gas disk, then it is more compact than many other ULIRG disks (Downes & Solomon 1998). However, systematic effects may impact the determination of the disk size from NIR tracers (e.g., the heavy nuclear extinction in this galaxy). CO or other cold molecular gas observations would be more conclusive.

The disk kinematics are shown in Figure 2. H II and H_2 tracers of the disk yield similar results, but the H II tracers have higher signal-to-noise ratio and allow the disk to be traced to larger radius. We thus show only the Paα kinematics. A rotating ionized disk of at least 3 kpc radius had already been detected (RV13). The systemic redshifts determined from Paα ($z = 0.0583$) and optical emission lines (0.0584; RV13) are identical within the errors.

The kinematics at small scales show a slight misalignment of the line of nodes compared to that at larger scales. The Hα velocities at radii >1 kpc have an apparent disk line of nodes of $(120 \pm 10)^\circ$ (RV13). At smaller scales the isovelocity contours twist. The compact Paα disk has a line of nodes of $(140 \pm 10)^\circ$ at radii $\lesssim$200 pc. This kinematic misalignment could arise from a disk warp or under the influence of stellar structures such as a bar or oval distortion (Emsellem et al. 2006; Riffel & Storchi-Bergmann 2011).

The second molecular gas component is broad and blueshifted (Figures 2 and 3). It extends directly along the galaxy minor axis from 100 to 400 pc NE of the nucleus. The mean velocity in this component (which we label $v_{50\%}$, meaning that 50% of the gas covered by a spaxel is less blueshifted than this velocity) decreases with increasing radius from -700 km s^{-1} at radii <200 pc to -1000 km s^{-1} at radii >300 pc, while the FWHM declines from 700 km s^{-1} to 500 km s^{-1}. To describe the most blueshifted velocities, we use $v_{98\%} \equiv v_{50\%} - 2\sigma$, meaning that 98% of the gas covered by a spaxel is less blueshifted than this velocity. The value of $v_{98\%}$ remains fairly constant with radius, with a mean of -1300 km s^{-1} and a range of -1000 to -1700 km s^{-1}. However, given the noise in the line wings in individual spaxels, the actual velocities may not reach -1700 km s^{-1}. The integrated line profile reaches velocities of

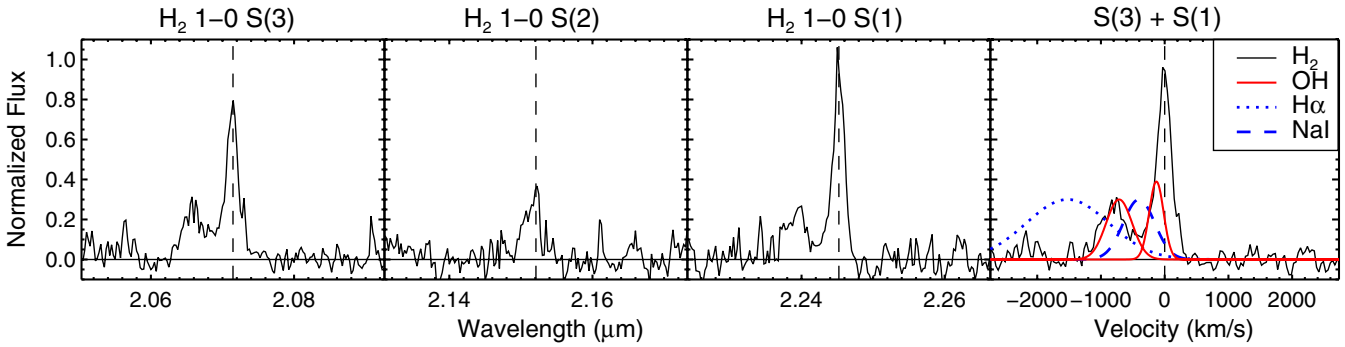

Figure 3. NIR H_2 profiles in F08572+3915:NW. From left to right: H_2 1−0 S(3), H_2 1−0 S(2), H_2 1−0 S(1), and the sum of the H_2 1−0 S(3) and H_2 1−0 S(1) emission line profiles, summed over those spaxels in which a broad, blueshifted component is detected. In the rightmost panel, we overplot the two components of the OH velocity profile as solid red lines (Veilleux et al. 2013) and the spatially averaged Hα and Na I D outflow velocity profiles as dotted and dashed blue lines (RV13). There is excellent correspondence between the high-velocity H_2 and OH components. The ionized gas is overall more blueshifted. The neutral gas is lower in velocity, but it arises from a different location.

(A color version of this figure is available in the online journal.)

-1300 km s^{-1} (Figure 3). We conclude that the most blueshifted warm H_2 gas velocity is between -1300 and -1700 km s^{-1}.

F08572+3915:NW was previously known to host a molecular outflow, based on blueshifted OH absorption lines (Sturm et al. 2011; Veilleux et al. 2013). In Figure 3, we plot the two components of the OH profile (as fit in Veilleux et al. 2013) on top of the H_2 profile (integrated over the outflow region). There is excellent agreement in the velocities of the blueshifted OH and H_2 components. The low-velocity OH component traces the blue wing of the narrow H_2 component.

We conclude that the broad, blueshifted H_2 component in this galaxy is a minor axis molecular outflow. We observe only one side of the outflow, and infer that the counter-propagating side of the flow is hidden by the galaxy disk. The H_2 line intensity declines away from the galaxy nucleus and is highest through the bisector of the outflow cone (Figure 1). The increase of average velocity with radius (Figure 2) may result from a velocity segregation (high velocity gas reaching large radii more quickly than low velocity gas), rather than reflecting acceleration of the flow (Dalla Vecchia & Schaye 2008).

The (one-sided) wind opening angle inferred from our data is $(100 \pm 10)^\circ$ (Figure 2). This is smaller than the typical one-sided opening angle inferred from OH or Na I D surveys (Veilleux et al. 2013; Rupke et al. 2005). These surveys yield a detection rate of 70%, which imply a (one-sided) conical opening angle of 145°. Similarly, preliminary modeling of the OH line in F08572+3915:NW yields an opening angle of ∼150° (Sturm et al. 2011).

The H_2 1−0 S(3)/H_2 1−0 S(1) and H_2 1−0 S(3)/H_2 1−0 S(2) line ratios in the disk yield median temperatures of 1700 K and 1300 K, respectively. If this emission is thermal in origin, then these temperatures could be made consistent with a reduction in the ortho-to-para ratio from 3.0 to 2.1–2.2 (Smith et al. 1997). The H_2 1−0 S(3)/H_2 1−0 S(1) line ratio in the outflow shows a median excitation temperature of 2370 K. This temperature is higher than in the disk (a K-S test shows that the disk and outflow temperature distributions differ at the 96% level).

The next levels of rotational-vibrational excitation of H_2 in our wavelength range are the 1−0 S(4) line and the 2−1 lines. Systemic 1−0 S(4) is detected in our spectra, but it lies at the bottom of a strong telluric feature. In integrated spectra, it has a similar flux to the 1−0 S(2) line. The brightest 2−1 line is likely H_2 2−1 S(3) at 2.07 μm. The integrated spectrum yields an upper limit of 0.2 for the $H_2$2−1 S(3)/H_2 1−0 S(1) line ratio.

4. DISCUSSION

This data set on F08572+3915:NW is significant for two reasons. First, it shows a high spatial resolution view of a molecular outflow driven by a QSO in a galaxy merger. It is thus one of the handful of such molecular outflows that is resolved, and the only one resolved at sub-kiloparsec scales. Second, it may be an example of AGN feedback in action: a deeply buried QSO that is in the process of removing the dusty molecular gas that obscures it.

Neutral atomic, ionized, and molecular gas outflows have been detected in other studies of F08572+3915:NW (Sturm et al. 2011; RV13; Cicone et al. 2013). At a resolution of 1 kpc, the ionized gas is elongated along the minor axis of the galaxy, and it has the highest outflow velocities (peaking at 3350 km s^{-1}) among six major mergers studied with IFS (RV13). As observed in both single aperture spectra of OH and in CO emission with a resolution of several kiloparsecs, the outflowing gas has a peak velocity of 700–800 km s^{-1} and a maximum velocity ($v_{98\%}$) of 1100–1200 km s^{-1} (Sturm et al. 2011; Veilleux et al. 2013; Cicone et al. 2013). Finally, high-excitation CO absorption has been detected at blueshifts up to -400 km s^{-1} (Geballe et al. 2006; Shirahata et al. 2013).

Besides the improved spatial resolution, this data set represents one of the few resolved observations of a molecular outflow in major mergers or QSOs. *Herschel* observations of molecular outflows in ULIRGs are spatially unresolved (Sturm et al. 2011; Veilleux et al. 2013), and previous CO observations of ULIRGs or QSOs have resolved molecular outflows in only a few cases (Feruglio et al. 2010; Aalto et al. 2012; Cicone et al. 2012; Feruglio et al. 2013; Cicone et al. 2013). Most of the CO outflows in these systems are asymmetric, with the blue and/or red wing extended to one side, while in NGC 6240 the extended CO gas is in filaments that are co-spatial with extended warm and hot ionized gas structures.

In F08572+3915:NW, we determine that the molecular wind is collimated by the nuclear disk along the minor axis of the system. The same was found for the ionized gas in this galaxy, and more generally in other mergers on scales up to 2 kpc (RV13). A one-sided, limb-brightened superbubble is also seen in H_2 emission in NGC 4945 (e.g., Moorwood et al. 1996; Marconi et al. 2000). However, rather than being limb-brightened, the H_2 emission in the F08572+3915:NW outflow is concentrated near the outflow axis (Figure 1).

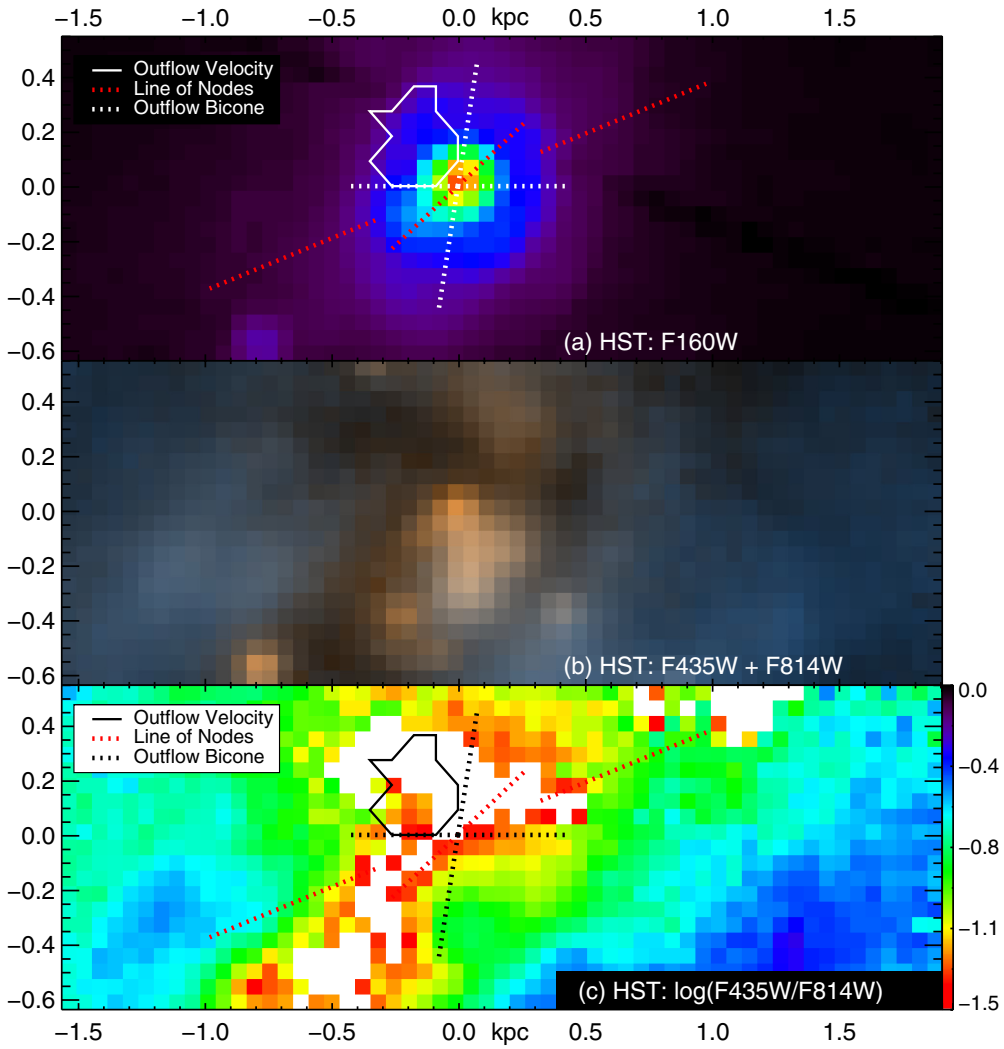

Figure 4. *Hubble Space Telescope* images of F08572+3915:NW. From top to bottom, the images are NICMOS F160W, ACS WFC F435W+F814W, and log(F435W/F814W). In the bottom panel, white represents areas where the extinction is so heavy that the galaxy is not detected in F435W. In the top and bottom panels, we overlay the contours of the nuclear outflow velocity field, the disk line of nodes, and an estimate of the outflow's opening angle. The nuclear outflow is coincident with a plume of dust absorption.

(A color version of this figure is available in the online journal.)

Previous authors have concluded that the buried QSO in F08572+3915:NW plays a significant role in powering the outflow (Sturm et al. 2011; RV13; Veilleux et al. 2013). This conclusion was based on the high velocities observed (greater than outflow velocities observed in similar systems with no detected AGN), the high energy of the outflow (which requires an unreasonably high thermalization efficiency if the starburst alone powers the outflow), and the high momentum of the outflow.

The present data strengthen the case for a significant contribution from an AGN. Given its size, the outflow cannot emerge from a region much larger than ∼200 pc in diameter. It is consistent with emerging from a region that is even smaller. The mid-infrared continuum source in this system is very small (size <100 pc; Imanishi et al. 2011), and it is dominated by the buried AGN (Veilleux et al. 2009a). Furthermore, the inner gas disk, as traced by Paα and NIR H_2 lines, is apparently concentrated within the central 100–200 pc in radius (Section 3).

Given that we only detect the outflow securely in two molecular lines (Figure 3), it is difficult to constrain the gas excitation. However, the wind is more highly excited than the disk. Typically, NIR and MIR H_2 emission in ULIRG disks is consistent with originating in photodissociation regions (Davies et al. 2003; Higdon et al. 2006), though shock excitation may also play a role (van der Werf et al. 1993; Zakamska 2010).

Strikingly, the warm and cold molecular phases share very similar kinematics (Figure 3). Thus, it is plausible that the warm and cold molecular gas are cospatial. The warm H_2 could reside in the outer regions of dense clouds that are being externally heated.

To estimate the mass of warm H_2 in the outflow, we assume thermal equilibrium at $T = 2370$ K (Section 3). The H_2 1−0 S(3) flux is 1.1×10^{-15} erg s^{-1} cm^{-2}. The equations from Roussel et al. (2007) and the partition function from Herbst et al. (1996) give $N(H_2) = 1.8 \times 10^{19}$ cm^{-2} and $M(H_2, \mathrm{warm}) = 5.2 \times 10^4\ M_\odot$. This is a factor 1.6×10^3 lower than the mass in the neutral atomic and ionized phases of the wind (RV13). Based on our measured $v_{50\%} = -1000$ km s^{-1} at 400 pc, the dynamical time is 0.4 Myr, yielding a mass outflow rate of $dM/dt(H_2, \mathrm{warm}) = 0.13\ M_\odot\ \mathrm{yr}^{-1}$.

As determined from OH transitions, $dM/dt(H_2)$ is $1000^{+2900}_{-730}\ M_\odot\ \mathrm{yr}^{-1}$ (Sturm et al. 2011), while the ionized and

neutral gas outflow rate is $30\,M_{\odot}\,\mathrm{yr}^{-1}$ (RV13). To bring the warm molecular outflow rates in line with other measured rates, the ratio of total to warm molecular gas in the F08572+3915:NW outflow must be lower than in the M82 wind by factors of 10–100 (Veilleux et al. 2009b). The different radiation environments and outflow speeds in the two galaxies may cause this difference.

Dust is present in the outflow in the form of an optically thick filament that wraps around the edge of the H_2 emission (Figure 4). This plausibly implies that the molecular outflow is beginning to excavate dust from around the AGN, and will uncover the QSO on short timescales. This molecular flow may thus be a missing link between the buried and naked QSO phases in the classic major merger timeline (Sanders et al. 1988; Hopkins et al. 2005). The outflow in the nearby QSO Mrk 231, which has reached scales of several kpc (Rupke & Veilleux 2011) may be a prime example of the next phase: a true QSO with a large scale galactic wind that has already done its work.

The authors thank the referee for a helpful report. D.S.N.R. was supported by a NASA Keck PI Data Award, administered by the NASA Exoplanet Science Institute, and by a Cottrell College Science Award. S.V. acknowledges NSF support under grant AST-10009583. Data presented herein were obtained at the W. M. Keck Observatory from telescope time allocated to NASA. The Observatory was made possible by the generous financial support of the W. M. Keck Foundation. The *HST* observations described herein were obtained from the Hubble Legacy Archive.

REFERENCES

Aalto, S., Garcia-Burillo, S., Muller, S., et al. 2012, A&A, 537, A44
Armus, L., Charmandaris, V., Bernard-Salas, J., et al. 2007, ApJ, 656, 148
Cicone, C., Feruglio, C., Maiolino, R., et al. 2012, A&A, 543, A99
Cicone, C., Maiolino, R., Sturm, E., et al. 2013, A&A, submitted
Crenshaw, D. M., & Kraemer, S. B. 2012, ApJ, 753, 75
Dalla Vecchia, C., & Schaye, J. 2008, MNRAS, 387, 1431
Davies, R. I., Sternberg, A., Lehnert, M., & Tacconi-Garman, L. E. 2003, ApJ, 597, 907
Downes, D., & Solomon, P. M. 1998, ApJ, 507, 615
Emsellem, E., Fathi, K., Wozniak, H., et al. 2006, MNRAS, 365, 367
Feruglio, C., Fiore, F., Maiolino, R., et al. 2013, A&A, 549, A51
Feruglio, C., Maiolino, R., Piconcelli, E., et al. 2010, A&A, 518, L155
Fischer, J., Sturm, E., Gonzlez-Alfonso, E., et al. 2010, A&A, 518, L41
Geballe, T. R., Goto, M., Usuda, T., Oka, T., & McCall, B. J. 2006, ApJ, 644, 907
Herbst, T. M., Beckwith, S. V. W., Glindemann, A., et al. 1996, AJ, 111, 2403
Higdon, S. J. U., Armus, L., Higdon, J. L., Soifer, B. T., & Spoon, H. W. W. 2006, ApJ, 648, 323
Hopkins, P. F., & Elvis, M. 2010, MNRAS, 401, 7
Hopkins, P. F., Hernquist, L., Cox, T. J., et al. 2005, ApJ, 630, 705
Imanishi, M., Imase, K., Oi, N., & Ichikawa, K. 2011, AJ, 141, 156
Larkin, J., Barczys, M., Krabbe, A., et al. 2006, Proc. SPIE, 6269, 42
Marconi, A., Oliva, E., van der Werf, P. P., et al. 2000, A&A, 357, 24
Moorwood, A. F. M., van der Werf, P. P., Kotilainen, J. K., Marconi, A., & Oliva, E. 1996, A&A, 308, L1
Riffel, R. A., & Storchi-Bergmann, T. 2011, MNRAS, 411, 469
Roussel, H., Helou, G., Hollenbach, D. J., et al. 2007, ApJ, 669, 959
Rupke, D. S., Veilleux, S., & Sanders, D. B. 2005, ApJS, 160, 115
Rupke, D. S. N., Kewley, L. J., & Chien, L. 2010, ApJ, 723, 1255
Rupke, D. S. N., & Veilleux, S. 2011, ApJL, 729, L27
Rupke, D. S. N., & Veilleux, S. 2013, ApJ, 768, 75
Sanders, D. B., Soifer, B. T., Elias, J. H., et al. 1988, ApJ, 325, 74
Scoville, N. Z., Evans, A. S., Thompson, R., et al. 2000, AJ, 119, 991
Shirahata, M., Nakagawa, T., Usuda, T., et al. 2013, PASJ, 65, 5
Smith, M. D., Davis, C. J., & Lioure, A. 1997, A&A, 327, 1206
Soifer, B. T., Neugebauer, G., Matthews, K., et al. 2000, AJ, 119, 509
Sturm, E., Gonzlez-Alfonso, E., Veilleux, S., et al. 2011, ApJL, 733, L16
Tokunaga, A. T., & Vacca, W. D. 2005, PASP, 117, 421
van der Werf, P. P., Genzel, R., Krabbe, A., et al. 1993, ApJ, 405, 522
Veilleux, S., Melendez, M., Sturm, E., et al. 2013, ApJ, in press
Veilleux, S., Rupke, D. S. N., Kim, D.-C., et al. 2009a, ApJS, 182, 628
Veilleux, S., Rupke, D. S. N., & Swaters, R. 2009b, ApJL, 700, L149
Westmoquette, M. S., Clements, D. L., Bendo, G. J., & Khan, S. A. 2012, MNRAS, 424, 416
Zakamska, N. L. 2010, Natur, 465, 60

The Astrophysical Journal Letters, 827:L20 (3pp), 2016 August 10 doi:10.3847/2041-8205/827/1/L20
© 2016. The American Astronomical Society. All rights reserved.

ERRATUM: "BREAKING THE OBSCURING SCREEN: A RESOLVED MOLECULAR OUTFLOW IN A BURIED QSO" (2013, ApJL, 775, L15)

David S. N. Rupke[1] and Sylvain Veilleux[2]
[1] Department of Physics, Rhodes College, Memphis, TN 38112, USA; drupke@gmail.com
[2] Department of Astronomy and Joint Space-Science Institute, University of Maryland, College Park, MD 20742, USA
Received 2016 July 20; published 2016 August 10

In the published article, the data cube was incorrectly flipped about one spatial axis. There are three consequences of this, none of which affect the conclusions of the Letter. First, the molecular outflow now points to the SE, instead of the NE (Figure 1). Second, the line of nodes of the compact Paα disk is now 60°, rather than 140° (Figure 2). This increases the misalignment of the small-scale

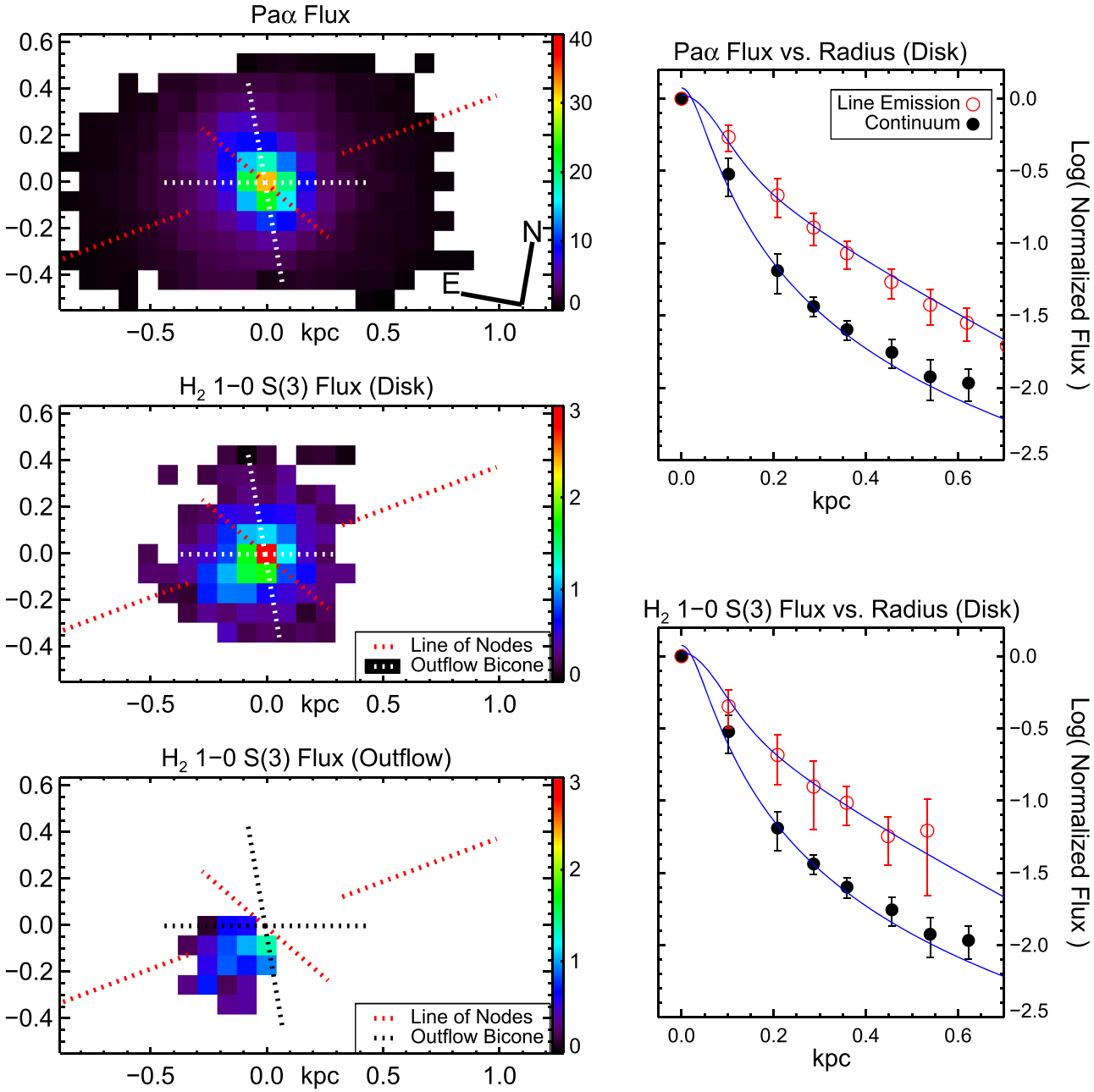

Figure 1. Left: flux maps of the gas disk and outflow in F08572+3915:NW, in units of 10^{-16} erg s^{-1} cm^{-2}. The top two maps shows Paα and H_2 1-0 S(3) in the disk and the bottom map shows H_2 1-0 S(3) in the outflow. The red dotted lines show the approximate lines of nodes of the inner (60° east of north) and outer (120°) disks, while the black and white dotted lines outline a possible biconical shape for the wind (of one-sided opening angle 100°. (For comparison, continuum and dust images appear in Figure 4.) Right: flux vs. radius in 0.″07 radial bins. Black filled circles show the 2.0–2.2 μm continuum; red open circles show line emission; and error bars represent dispersion. The blue line through the continuum data is a Moffat fit (FWHM = 0.″09). The blue line through the emission line data is a Gaussian + exponential model.

line of nodes with the line of nodes on large scales; this misalignment is relevant only to the interpretation of the disk kinematics, which is not part of this Letter. Third, the orientation of the outflow with respect to the optical dust features changes (Figure 4). The outflow is still bordered by an optically thick dust filament, as pointed out in the published article, though now it is a different filament.

The impacted Figures 1, 2, and 4 are shown here with corrections applied. In Figures 1 and 2, the maps, velocity contours, small-scale line of nodes, and outflow bicone are flipped vertically. In Figure 4, the outflow velocity contour, small-scale line of nodes, and outflow bicone are flipped vertically.

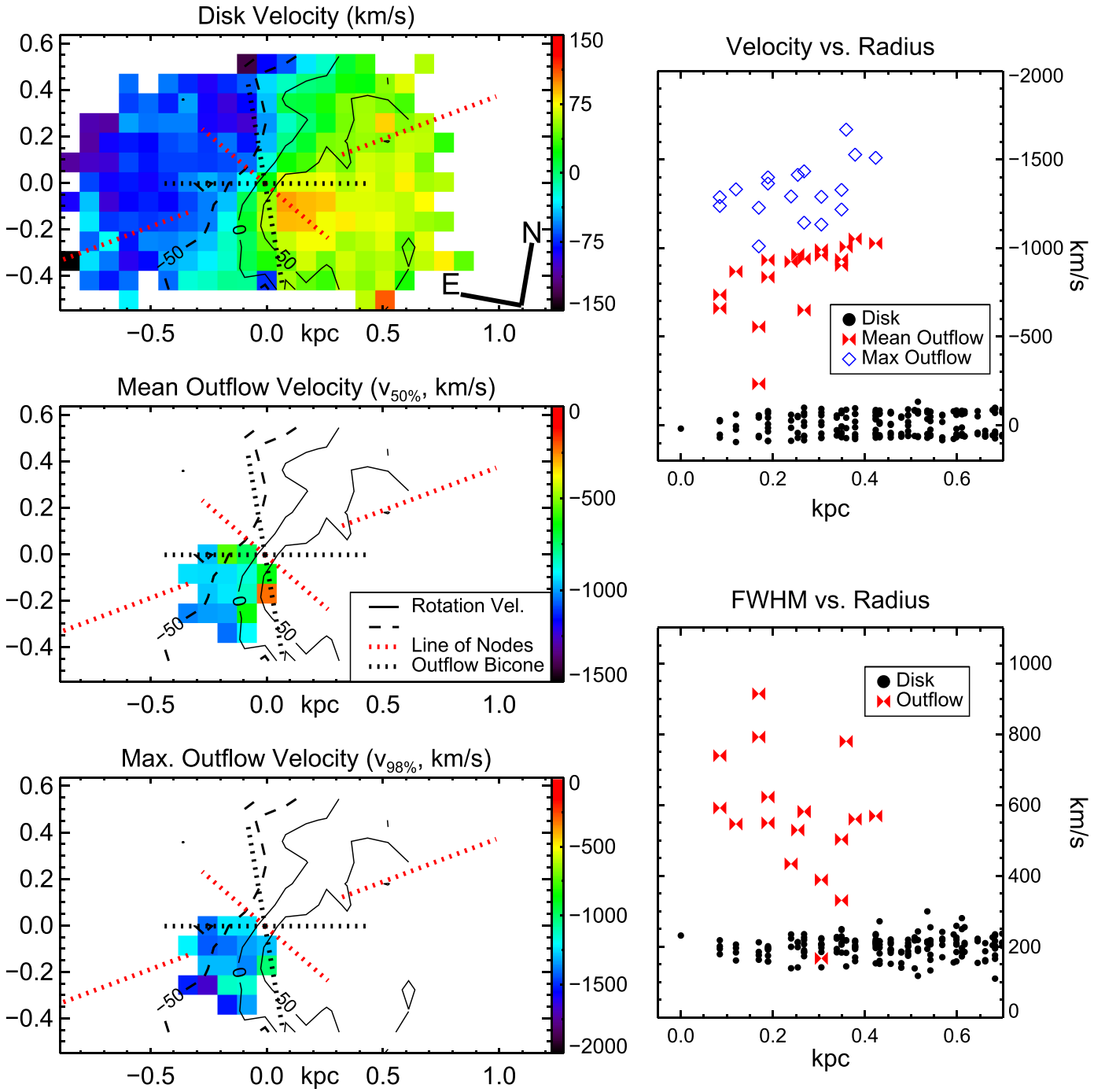

Figure 2. Left: velocity maps of rotation and outflow in F08572+3915:NW, with respect to $z = 0.0583$. From top to bottom: ionized gas rotation, mean outflow velocity ($v_{50\%}$) in H_2, and maximum outflow velocity ($v_{98\%}$) in H_2. The red and black dotted lines are the same as in Figure 1. The blueshifted component extends along the minor axis of the nuclear disk. Right: velocity and FWHM vs. radius. Black filled circles represent velocity and FWHM of rotating components (Paα), red filled hourglasses show mean outflow velocity and outflow FWHM (H_2), and blue open diamonds show maximum outflow velocity. The outflow is more blueshifted with increasing radius, while the FWHM declines.

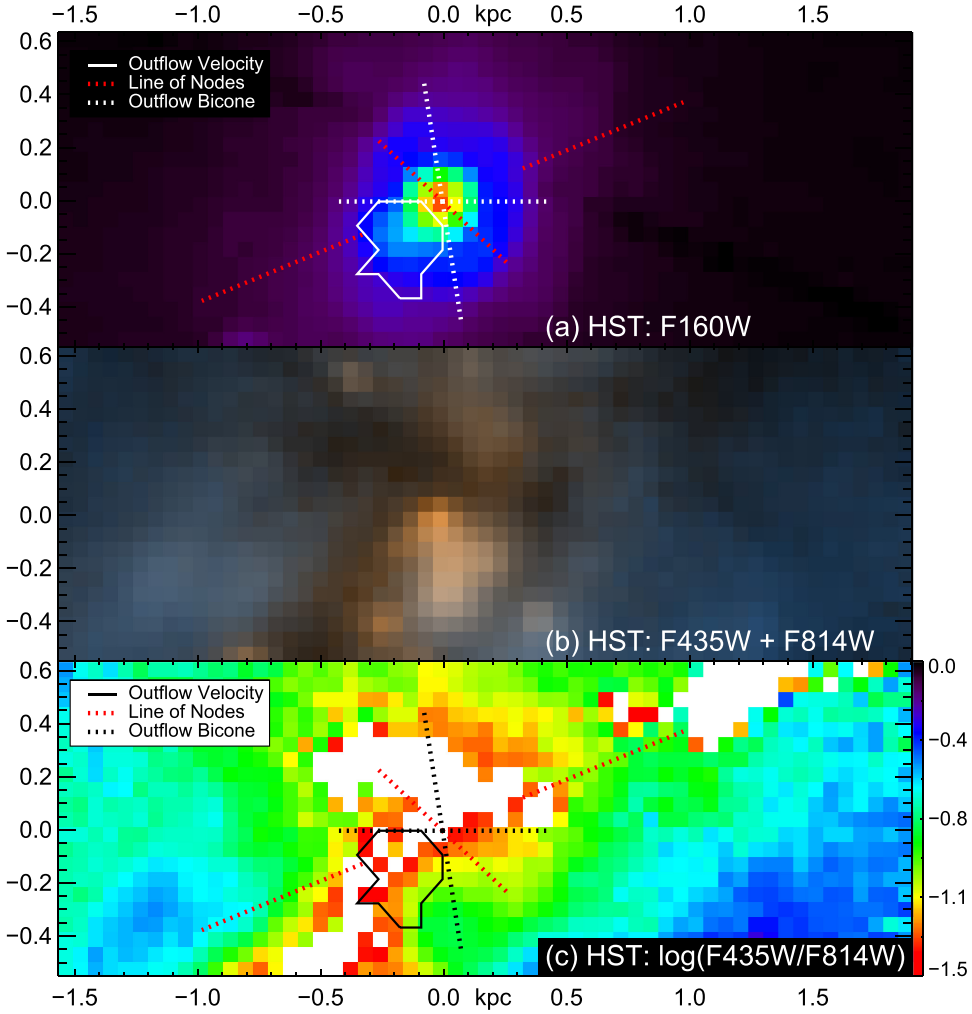

Figure 4. *Hubble Space Telescope* images of F08572+3915:NW. From top to bottom, the images are NICMOS F160W, ACS WFC F435W+F814W, and log (F435W/F814W). In the bottom panel, white represents areas where the extinction is so heavy that the galaxy is not detected in F435W. In the top and bottom panels, we overlay the contours of the nuclear outflow velocity field, the disk line of nodes, and an estimate of the outflow's opening angle. The nuclear outflow is coincident with a plume of dust absorption.